

# Cohesive model for crack propagation analyses of structures with elastic–plastic material behavior

## Foundations and implementation

Ingo Scheider  
GKSS research center Geesthacht, Dept. WMS

April 2001

### **Abstract**

In this document the cohesive model, a phenomenological model for crack propagation analyses, is presented. An implementation of the model exists at GKSS for several years and is developed steadily, therefore the foundations are explained first, and details specific to the actual implementation as a user defined element within the FE system ABAQUS are described afterwards.

The actual paper describes the implemented version of the user subroutine, which contains traction-separation-laws of Needleman, [Needleman, 1990], which is used for example in [Siegmund and Brocks, 1998], [Tvergaard, 1990] and Scheider, [Scheider, 2001a], used also in [Scheider, 2001b]. A guide for the practical use of the cohesive model and the determination of the material parameters is outside the scope of this document and will be published in a separate paper.

# Nomenclature

$\Gamma$	cohesive energy
$\Gamma_0$	critical cohesive energy at failure of the cohesive element
$\Phi$	potential of separation stress
$\Pi_i$	inner energy
$\alpha$	connection parameter between normal- and tangential stress and – separation, respectively
$\delta$	separation (displacement jump between upper and lower side of the cohesive element)
$\delta^N, \delta^T$	normal and tangential portion of the separation, resp.
$\delta_0$	critical separation at failure
$D$	dimensionless damage parameter
$\mathbf{K}$	stiffness matrix
$J$	crack driving force parameter
$J_i$	$J$ -integral at crack initiation
$\mathbf{J}$	Jakobi matrix
$T$	cohesive stress
$T_0$	max. cohesive stress
$T^N, T^T$	normal and tangential portion of the cohesive stress
$\mathbf{V}_{\mathbf{u}}$	matrix of shape functions
$\mathbf{f}$	vector of nodal forces
$\mathbf{g}_i$	basis of local coordinate system
$\mathbf{t}$	cohesive stress vector at nodes
$\mathbf{u}$	displacement vector
$[\mathbf{u}]$	displacement jump vector in the cohesive element ( $\equiv$ separations)

# Contents

<b>1</b>	<b>Introduction</b>	<b>3</b>
<b>2</b>	<b>Mechanics of cohesive models</b>	<b>5</b>
2.1	Advanced cohesive models . . . . .	5
2.2	Traction separation law, TSL . . . . .	7
2.3	Consideration of normal and shear fracture . . . . .	7
2.4	Unloading . . . . .	9
2.4.1	Normal separation . . . . .	10
2.4.2	Tangential separation . . . . .	11
2.5	Consideration of contact and friction . . . . .	12
<b>3</b>	<b>Implementation</b>	<b>15</b>
3.1	Form of the TSL . . . . .	15
3.1.1	Polynomial TSL . . . . .	15
3.1.2	Exponential TSL . . . . .	16
3.1.3	Partly constant TSL . . . . .	17
3.1.4	Aspects of numerical implementation . . . . .	20
3.2	Element library . . . . .	21
3.3	Local coordinate system . . . . .	22
3.4	Energy principle for the cohesive element . . . . .	23
<b>4</b>	<b>ABAQUS input for the cohesive element</b>	<b>27</b>
<b>5</b>	<b>Results output</b>	<b>29</b>
<b>6</b>	<b>Three element test for tangential separation</b>	<b>31</b>
	<b>Bibliography</b>	<b>33</b>

<b>A Program structure</b>	<b>35</b>
A.1 For the 3D-cohesive elements: . . . . .	35
A.2 For the 2D cohesive elements: . . . . .	36
<b>B Inputfile for the verification example</b>	<b>37</b>

# Chapter 1

## Introduction

The idea for the cohesive model is based on the consideration that infinite stresses at the crack tip are not realistic. Models to overcome this drawback have been introduced by [Dugdale, 1960] and by [Barenblatt, 1962]. Both authors divided the crack in two parts: One part of the crack surfaces, region I in fig. 1.1, is stress free, the other part, region II, is loaded by cohesive stresses. Dugdale introduced the finite stress to be the yield stress, which holds only for plane stress, but the crack opening stresses can be much higher than the equivalent stress in a multiaxial stress state. Barenblatt, who investigated the fracture of brittle materials, made several assumptions about the cohesive stresses: The extension of the cohesive zone  $d$  is constant for a given material (independent from global load) and small compared to other dimensions. The stresses in the cohesive zone follow a prescribed distribution  $\sigma(x)$ , where  $x$  is the ligament coordinate, which is specific for a given material but independent of the global loading conditions.

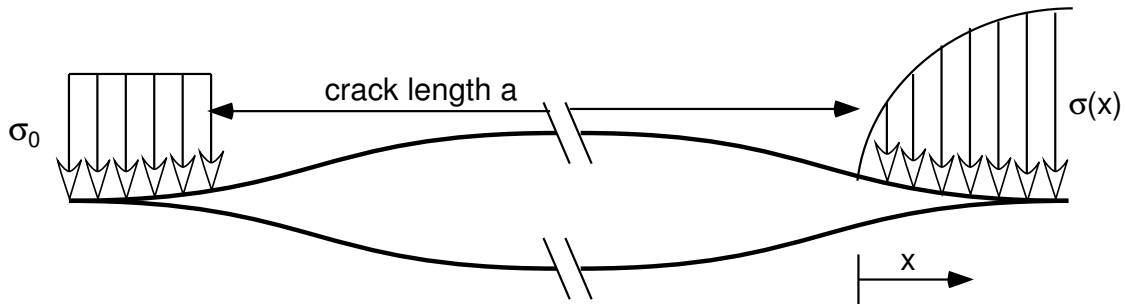


**Fig. 1.1:** Dugdale (left) and Barenblatt (right) crack models

Contrary to computational crack propagation analyses using the Gurson model, [Gurson, 1977], and modifications due to [Tvergaard, 1990], respectively, no continuum elements are damaged in the cohesive model. Cohesive interface elements are defined between the continuum elements instead, which open when damage occurs and lose their stiffness at failure so that the continuum elements are disconnected. For this reason the crack can propagate only along the element boundaries. If the crack propagation direction is not known in advance, the mesh generation has to make different crack paths possible.

In chapter 2 the mechanical behavior of a cohesive zone is explained. The implementation of the cohesive zone as user defined elements in the FE system ABAQUS is described in chapter 3.



## Chapter 2

# Mechanics of cohesive models

### 2.1 Advanced cohesive models

Most of the recently developed and proposed models are different from Barenblatt's model in that they define the traction acting on the ligament in dependency to the opening and not to the crack tip distance as Barenblatt did.

For practical applications the model became more interesting when numerical methods, mostly the finite element method, were applicable to nonlinear problems. [Needleman, 1987] was the first, who used the model for crack propagation analyses of ductile materials. More than ten years earlier [Hillerborg et al., 1976] applied the cohesive model to brittle fracture using the finite element method for the first time, followed already in the 80's by [Pettersson, 1981] and [Carpinteri, 1986] amongst others.

The material separation und thus damage of the structure is classically described by interface elements — no continuum elements are damaged in the cohesive model. Using this technique, the behavior of the material is split in two parts, the damage-free continuum with an arbitrary material law, and the cohesive interfaces between the continuum elements, which specify only the damage of the material.

The interface elements open when damage occurs and loose their stiffness at failure so that the continuum elements are disconnected. For this reason the crack can propagate only along the element boundaries. If the crack propagation direction is not known in advance, the mesh generation has to make different crack paths possible.

The separation of the cohesive interfaces is calculated from the displacement jump  $[\mathbf{u}]$ , i.e. the difference of the displacements of the adjacent continuum elements,

$$\delta = [\mathbf{u}] = \mathbf{u}^+ - \mathbf{u}^-. \quad (2.1)$$

More common than the definition of the separation vector in global coordinates is the description in a local coordinate system, namely the distinction between normal separation,  $\delta^N$ , and tangential separation,  $\delta^T$  as shown in fig. 2.1. The separation depends on the normal and the shear stress, respectively, acting on the surface of the interface. When the normal or tangential component of the separation reaches a critical value,  $\delta_0^N$  or  $\delta_0^T$ , respectively, the continuum

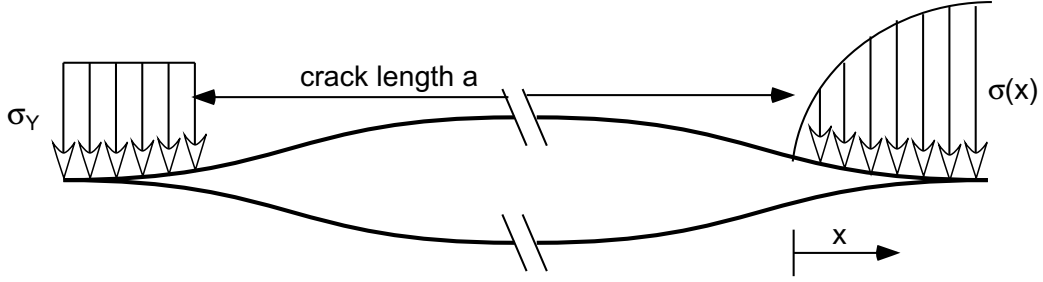


**Fig. 2.1:** Separation of 2D continuum elements connected by a cohesive interface.

elements initially connected by this cohesive element, are disconnected, which means that the material at this point has failed.

For three-dimensional problems, two tangential separation directions exist, which will be denoted as  $\delta^{T1}$  and  $\delta^{T2}$ . If isotropic materials are considered, a distinction between these two direction is not necessary. For the sake of simplicity one may define a resultant tangential separation by

$$\delta^T = \sqrt{\delta^{T1^2} + \delta^{T2^2}} \leq \delta_0^T, \quad (2.2)$$

which is physically meaningful if both components are monotonously increasing, at least. Generally, it can happen however, that the cohesive surfaces slide without changing the absolute tangential separation defined by eq. (2.2), which is a physically questionable assumption. For further considerations on unloading of cohesive elements see `kaprefunload`.

Beside the critical separation,  $\delta_0$ , the maximum traction (stress at the surface of the continuum element),  $T_0$ , is used as a fracture parameter, also denoted as 'cohesive strength'. The value of  $T_0$  only describes the maximum value of a traction-separation curve  $T(\delta)$ , in the following denoted as cohesive law. Like the separations, the stresses  $T$  can also act in normal or in tangential direction, leading to normal or shear fracture, respectively. The shape of the curve,  $T(\delta)$ , which is assumed to be a material independent cohesive law, is defined differently by various authors. Common to all cohesive laws is that

1. They contain the two material parameters  $T_0$  and  $\delta_0$  mentioned above and
2. for total failure the stresses become zero,  $T(\delta > \delta_0) \equiv 0$  for both normal and tangential separation (this condition is not fulfilled exactly for all cohesive laws as will be shown later).

Several cohesive laws (also called traction-separation laws, or decohesion laws) will be given in chapter 2.2.

The integration of the traction over separation, either in normal or in tangential direction, gives the energy dissipated by the cohesive elements,  $\Gamma_0$ . This third parameter can be determined from the former two by

$$\Gamma_0 = \int_0^{\delta_0} T(\delta) d\delta \quad (2.3)$$



and used alternatively to  $\delta_0$ .

One can show that the energy at failure  $\Gamma_0$  equals the Rice integral [Rice, 1968] of crack driving force  $J$  at initiation under the assumptions made for the validity of the HRR field [de Andres et al., 1999]. Therefore the parameter can be easily determined by experiments.

If both separation modes, the tangential and the normal separation, occur simultaneously, there is an influence of the normal separation on the tangential tractions and vice versa. The description for this case of 'mixed mode' and the basic assumptions made in the literature, is given in chapter 2.3. Other special issues are the unloading behavior of the cohesive zone and the sliding of a failed cohesive element under negative normal separation, what involves contact of the fracture surfaces, described in chapter 2.4.

The verification of the cohesive model and its parameters is not performed in this document, since the model is validated by several examples, see e.g. [Siegmund et al., 1999] and [Lin et al., 1996]. Nevertheless, one simple 2-element example is conducted in chapter 6 showing the treatment of shearfracture with alternating loading direction.

## 2.2 Traction separation law, TSL

The form of the function  $T(\delta)$  given in eq. (2.3) is defined in the TSL. Since the cohesive model is a phenomenological model there is no evidence which form to take for  $T(\delta)$ . So it has to be assumed independent from the material as a model quality. In the literature one can find several approaches, some of them are shown in fig. 2.2. The implemented TSL's are the cubic form of [Needleman, 1987] with its extensions regarding shear fracture and unloading due to [Tvergaard, 1990] and the exponential curve from [Needleman, 1990]. In addition a TSL similar to the law with constant stress ([Schwalbe and Cornec, 1994]), first mentioned in [Scheider, 2001a], is developed and implemented. The mathematical foundations for the models are given in chapter 3.1.

Beside the form of the curve, which was assumed to be a model quantity, there are two material parameters, i.e. the maximum separation stress  $T_0$ , which has to be overcome for final fracture, and the separation at failure  $\delta_0$ . These quantities define the 'height' and the 'width' of the curve, and give (together with the function of the curve) the dissipated energy per cohesive element as a result. The damage, in the following denoted as  $D$ , is defined as the ratio of the actual to the maximum separation

$$D = \frac{\delta}{\delta_0} \quad . \quad (2.4)$$

## 2.3 Consideration of normal and shear fracture

Under consideration of simultaneously acting normal and shear fracture one has to define a new quantity for damage and failure. As mentioned before, failure occurs in a pure normal fracture when the separation exceeds the maximum separation  $\delta_0^N$ . At combined normal and shear fracture (local in the cohesive element) the quantity which defines failure contains a normal and a shear component, i.e. the shear damage will reduce the ductility in normal direction and vice

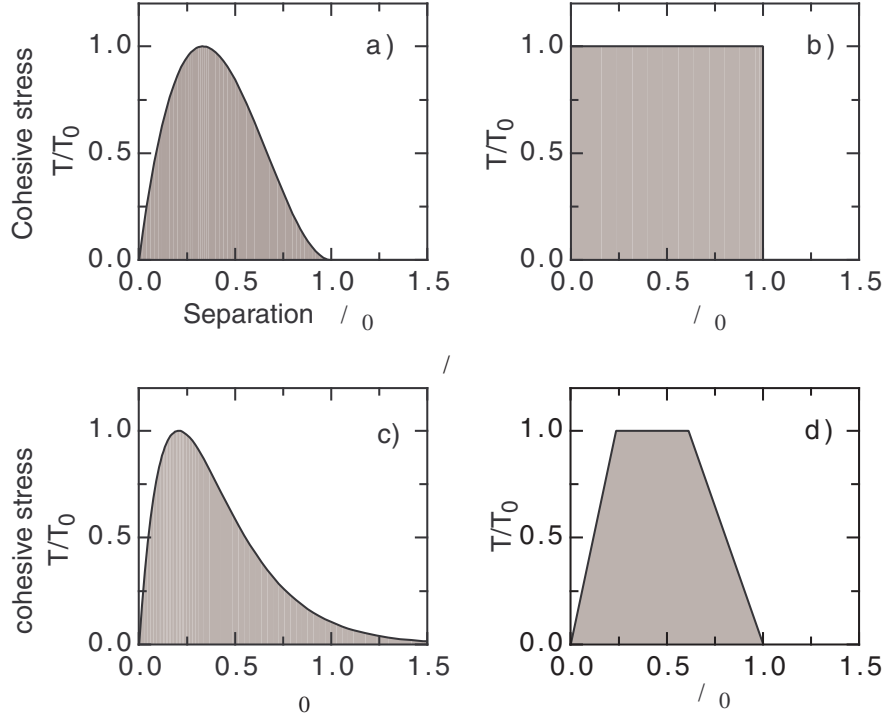


**Fig. 2.2:** Form of the TSL: a) cubic, from [Needleman, 1987], b) constant, from [Schwalbe and Cornec, 1994], c)exponential, from [Needleman, 1990], d) trilinear, from [Tvergaard and Hutchinson, 1992]

versa. This influence of competing normal and tangential separation is to define an interaction formula of the shear and normal separation:

$$D = \sqrt[m]{\left(\frac{\delta^N}{\delta_0^N}\right)^m + \left(\frac{\delta^T}{\delta_0^T}\right)^m} \quad (2.5)$$

Equation (2.5) contains a model parameter  $m$ , which is a connection parameter. One can determine two limiting cases from eq. (2.5), namely  $m = 1$ , that means a linear connection between normal and tangential damage, and  $m \rightarrow \infty$ , which leads to a vanishing influence of one fracture mode to another. The damage and final fracture of a cohesive element are plotted for  $m = 1$  and  $m = 2$  in fig. 2.3. It should be mentioned that most references use  $m = 2$  as the damage indicator, for which the damage is equal to the absolute value of separation.

As can be seen in the figure, the maximum normal separation decreases with increasing shear separation. Another way to embed the influence of tangential on normal opening (and vice versa) is to define the normal traction dependent on  $\delta^T$  explicitly. In both cases the separation function does not only depend on  $\delta^N$ , but also on  $\delta^T$  and/or on the damage  $D$ . Generally one can write for the TSL

$$T^N = T^N(\delta^N, D, \delta^T) \quad T^T = T^T(\delta^T, D, \delta^N) \quad (2.6)$$

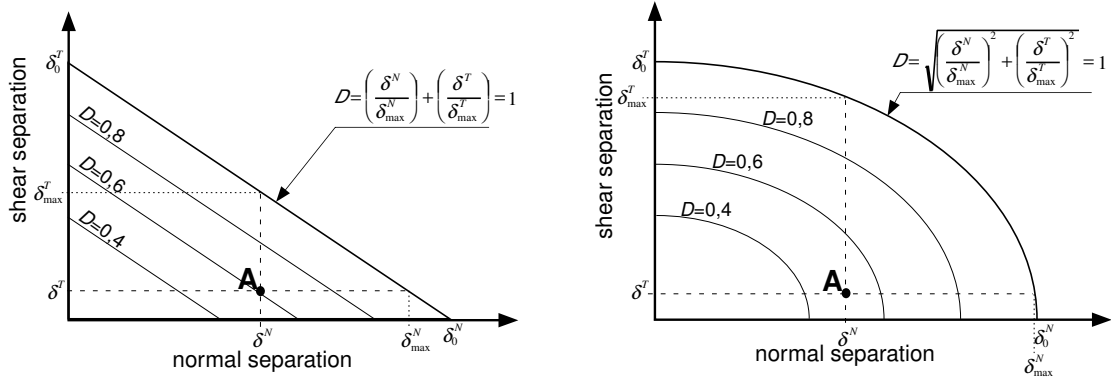


**Fig. 2.3:** Interaction between normal- and shear separation

We will see at the different implementations, chapter 3, that any implementation uses another dependence of the tractions on the separations.

## 2.4 Unloading

Local unloading effects can occur in the cases of global unloading of a structure, crack branching or multiple cracks. One has therefore to define the behavior of the cohesive elements under decreasing separation accounting for the irreversibility of the damage process. Since damage evolution is a nonlinear process as inelastic deformation, the cohesive models are established in analogy to the principles of plasticity, but allowing for strain softening. The terms 'loading' and 'unloading' will be used in the sense of increasing or decreasing separation, respectively, as the tractions decrease also under increasing separation beyond maximum stress,  $T_0$ . More generally, 'unloading' is any change of the deformation direction by which the stress state removes from the limiting traction-separation curve. The latter definition also applies for shear separation.

Two principle mechanisms depending on the material behavior have to be distinguished:

**Ductile unloading** The mechanical work for producing damage is totally dissipated, the void growth and hence the inelastic separation are irreversible and any reduction of separation occurs purely elastically with unchanged elastic stiffness, as shown in the upper row of fig. 2.4.

**Cleavage unloading** The elastic stiffness of the material is reduced by damage, but the separation vanishes when the stresses decrease to zero, as shown in the lower row of fig. 2.4.

Since the cohesive model is a phenomenological model, which can be used independently of the fracture mechanism, the two assumptions apply to different material behaviour. The first one is valid only for ductile crack propagation. Brittle fracture, which is characterized by micro cracks, would not be modelled correctly with a permanent separation on unloading, since the micro cracks close entirely (without getting back their stiffness). In this case the second unloading mechanism should be used.

A second important problem concerns loading and unloading under 'mixed mode' conditions, i.e. combined normal and tangential separation. Again, two different models can be considered:

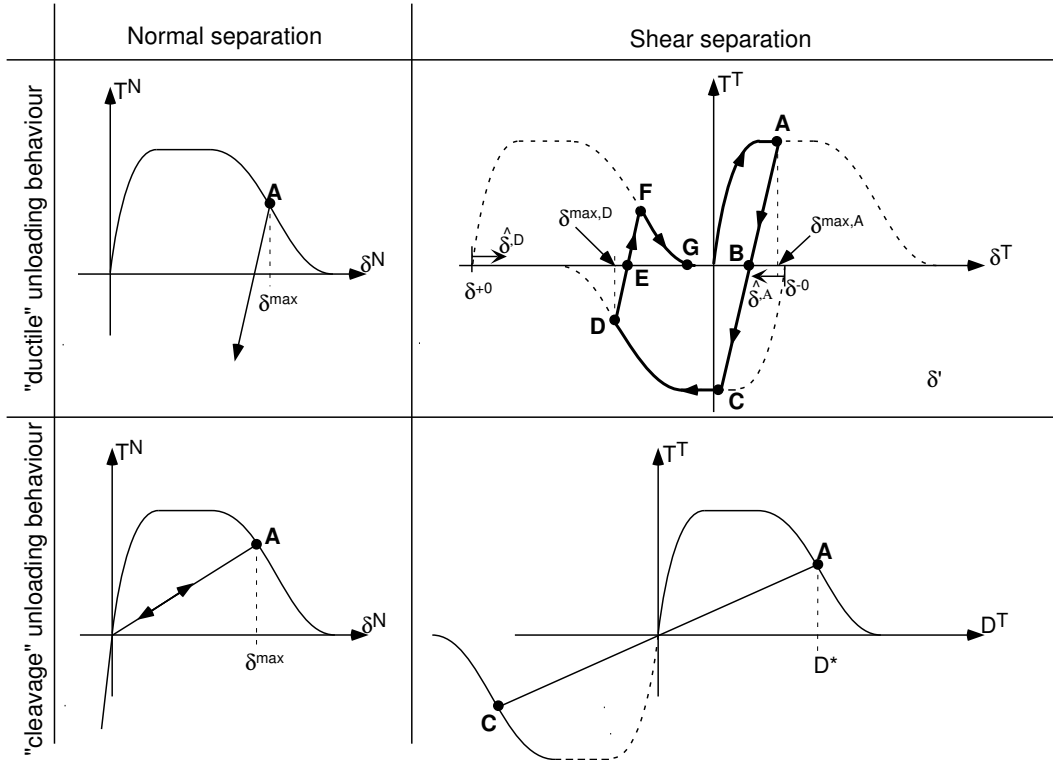


Fig. 2.4: Behavior of the TSL at unloading; a) normal separation, b) shear separation

- Unloading is handled separately for normal and tangential separation, i.e. a cohesive element can be in an unloading state for normal, but in a loading state for tangential separation and vice versa.
- Unloading depends on the total separation  $\delta = \sqrt{\delta^N{}^2 + \delta^T{}^2}$ . In this case unloading could be assumed even if the separation in one of the two modes might increase.

For pure normal or tangential separation both assumptions will lead to the same results. The behaviour of 'ductile' and 'cleavage' unloading are described further in the following subsections.

### 2.4.1 Normal separation

Under normal separation the difference between the two unloading mechanisms are shown on the left side of fig. 2.4. Up to the first unloading, which starts in Point **A**, there is no difference in the two mechanisms. In the unloading regime the traction separation correlation behaves differently as mentioned above and shown in the figure. In a new loading cycle (further increasing separation) first the separation stress increases on the same curve up to point **A** in the left figures of fig. 2.4 (both for "ductile" and "brittle" unloading mechanisms), and follows the original TSL afterwards.

Under local normal loading of a cohesive element the damage does not increase under compression but only under tension. If an initial tensile loading is reverted, the separation of the cohesive element behaves as shown in fig. 2.4. If the separation becomes negative, this means that the

two parts of the material are penetrating each other. In this case the stiffness of the cohesive element should be very high. for ductile fracture this condition is fulfilled automatically, but for cleavage fracture the stiffness must be increased if the normal separation  $\delta_0$  becomes negative.

The penetration of the cohesive surfaces must be checked even after total failure of the element, since a contact condition is further on acting between the surfaces, even though the element has no stiffness under conditions of positive separation.

### 2.4.2 Tangential separation

Under shear loading the damage can increase in both directions. It is assumed that a separation (and as a consequence: damage) which leads to dissipated energy in one direction is also active in the opposite direction, see the right side of fig. 2.4.

For the so-called "ductile" damage mechanism (upper right side of fig. 2.4), a new loading cycle leads to a more complex definition of the total shear damage definition: If the loading direction is changed at point **A** in the figure, then the dissipated energy remains lost (The cycle from the origin to point **A** is called *positive loading case*). After point **A**, where the total amount of separation is  $\delta^{max,A1}$ , the elastic unloading with a user defined stiffness similar to the unloading under normal separation comes into effect, called *positive unloading case*.

When the shear stress in the element becomes negative (point **B**), a new loading condition becomes effective, if the separation decreases further, but the TSL of the negative traction, the origin of which is shifted to  $\delta^{-0}$  due to already dissipated work, is not yet reached. This region is called *negative unloading case*, even though it is a loading condition, since it does not matter, whether the separation is on the way up or down the curve.

At point **C** the transformed TSL for the opposite direction is reached. It can be seen that the total separation is nearly zero even though a significant amount of work is already dissipated. Therefore an effective separation  $\hat{\delta}$  has to be defined, which has its origin in  $\delta^{-0}$ . The difference in separation between point **A** and **B** is called  $\delta^{back}$ , and thus the formulae for the origin of the negative TSL  $\delta^{-0}$  and the effective separation  $\hat{\delta}$  writes

$$\delta^{-0} = 2(\delta^{max,A} - \delta^{back}) \quad \text{and} \quad \hat{\delta} = \delta^{-0} - \delta^T \quad (2.7)$$

In all subsequent changes of the load cycles it is necessary to include the shift of the positive and the negative TSL's, as can be seen in the second change of the loading direction in fig. 2.4, after point **D**, where the calculation of the loading case depends on  $\delta^{-0}$  and the shift of the positive TSL,  $\delta^{+0}$ .

The flow diagram for the calculation of the shear tractions from the tangential separations is shown in fig. 2.5.

eq. (2.7) is valid when the direction switches only once. At an initially negative and a subsequent positive shear separation, not  $D^{-0}$  is shifted but  $D^{+0}$ . The transformed damage is then  $D_{trans} = D - D^{+0}$ . An example with multiple change in the loading direction can be find in chapter 6.

Up to now this unloading mechanism is only implemented for the 2D cohesive elements. An extension for 3D problems is planned.

---

<sup>1</sup>The index T for tangential separation is omitted here and in the following, since all separations in this section are tangential ones

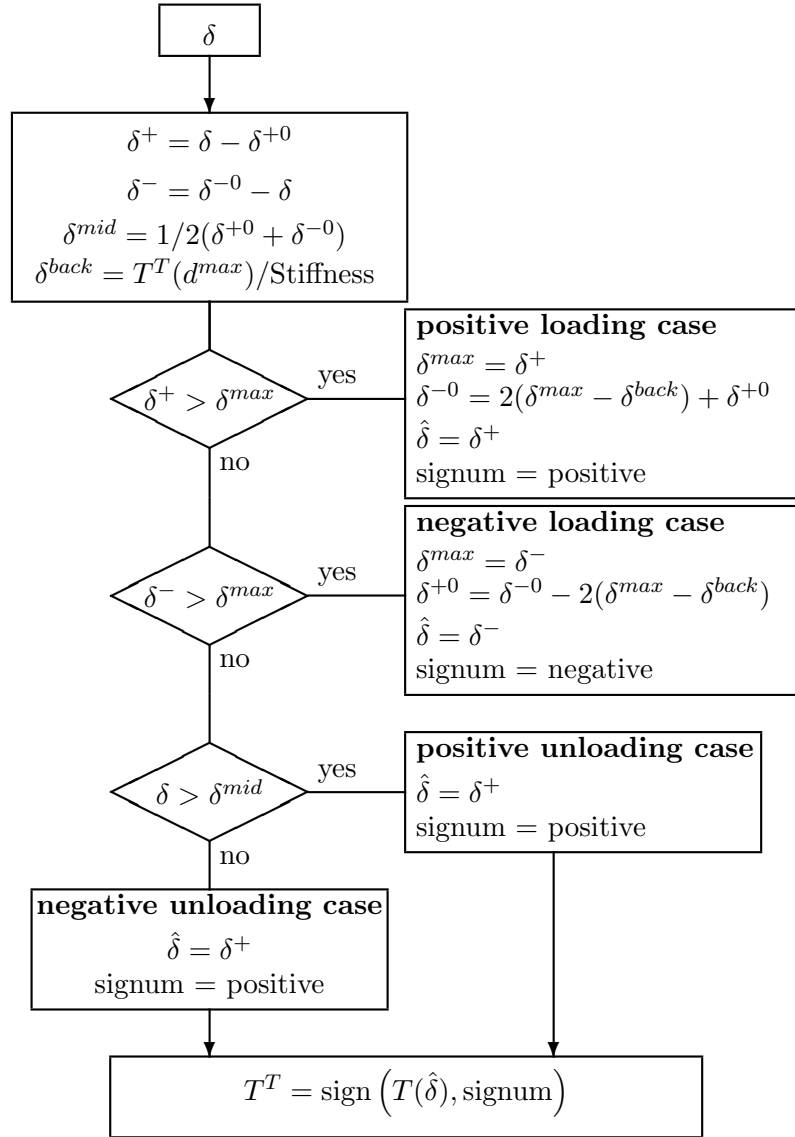


**Fig. 2.5:** Flowchart for the implementation of a "ductile" unloading mechanism. Notice that all separations are tangential separations.

## 2.5 Consideration of contact and friction

The contact condition of cohesive elements, i.e. prevention of adjacent continuum elements, has to be ensured also after total failure of the cohesive element. The behaviour after failure can be described as a contact TSL; depending on the mechanisms of ductile or brittle or ductile damage, respectively. This is illustrated in fig. 2.6 for the normal separation mode. The contact of failed cohesive elements is not yet implemented here. Further details can be found in [Roe, 2001].

If a structure fails under pure shear, frictional sliding of the fracture surfaces should be taken into account. The frictional forces can be integrated through an extension of the TSL. Since the determination of the friction coefficient of fracture surfaces is a difficult task and the parameter

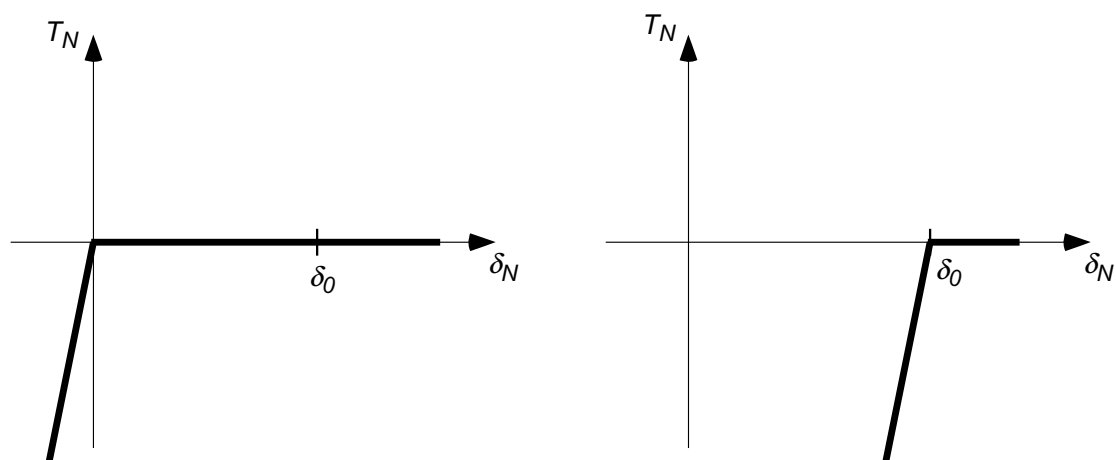


**Fig. 2.6:** Traction separation law of the cohesive element after failure for the consideration of contact.

changes significantly after a short distance of sliding, the sliding is not implemented in the cohesive model described in this paper. An approach for the consideration of frictional sliding can be found in [Chaboche et al., 1997]. One application where the effect is significant and must be regarded, is fiber pull-out in a composite material. The fracture mechanism in this case is pure shear.





## Chapter 3

# Implementation

### 3.1 Form of the TSL

The cohesive model has been implemented using the programming language FORTRAN as a *user defined element* within the FE code ABAQUS [Hibbitt et al., 1998]. The body of the user element routine was developed by T. Siegmund for twodimensional problems (lineshape cohesive elements). Two shapes of the TSL have been implemented in the original procedure: a polynomial function acc. to [Needleman, 1987], cf. fig. 2.2a) and an exponential function, acc. to [Needleman, 1990], see fig. 2.2c), respectively. Both stress functions are based on a potential. The polynomial function has been extended later, and a third TSL has been implemented based on [Scheider, 2001a].

#### 3.1.1 Polynomial TSL

The potential from which the stresses can be derived is for [Needleman, 1987]

$$\begin{aligned} \Phi = \frac{27}{4} T_0 \delta_0 & \left[ \frac{1}{2} \left( \frac{\delta^N}{\delta_0} \right)^2 \left( 1 - \frac{4}{3} \left( \frac{\delta^N}{\delta_0} \right) + \frac{1}{2} \left( \frac{\delta^N}{\delta_0} \right)^2 \right) + \dots \right. \\ & \left. \dots + \frac{1}{2} \alpha \left( \frac{\delta^T}{\delta_0} \right)^2 \left( 1 - 2 \left( \frac{\delta^N}{\delta_0} \right) + \left( \frac{\delta^N}{\delta_0} \right)^2 \right) \right] \end{aligned} \quad (3.1)$$

$\alpha$  is the ratio of normal to tangential stress or tangential to normal separation so that a constant separation energy  $\Gamma_0$  will be retrieved independently of the fracture mode. Equation (3.7) leads to the following stresses:

$$T^N = \frac{27}{4} T_0 \left[ \left( \frac{\delta^N}{\delta_0} \right) \left( 1 - 2 \left( \frac{\delta^N}{\delta_0} \right) + \left( \frac{\delta^N}{\delta_0} \right)^2 \right) + \alpha \left( \frac{\delta^T}{\delta_0} \right)^2 \left( \left( \frac{\delta^N}{\delta_0} \right) - 1 \right) \right] \quad (3.2)$$

and

$$T^T = \frac{27}{4} T_0 \alpha \left( \frac{\delta^T}{\delta_0} \right) \left( 1 - 2 \left( \frac{\delta^N}{\delta_0} \right) + \left( \frac{\delta^N}{\delta_0} \right)^2 \right) , \quad (3.3)$$

respectively. This model describes only debonding by normal separation and was then generalized by [Tvergaard, 1990], using the damage variable  $D$  of eq. (2.5) with an exponent  $m = 2$ . In addition, a "cleavage" unloading procedure has been implemented as described in chapter 2.4, in which the stiffness is reduced when damage occurs but separation totally vanishes when the traction is reduced to zero. The stresses are calculated by

$$T^N = \frac{27}{4} T_0^N \frac{\delta^N}{\delta_0^N} (1 - D_{\max})^2 \quad (3.4)$$

and

$$T^T = \frac{27}{4} T_0^T \frac{\delta^T}{\delta_0^T} (1 - D_{\max})^2 , \quad (3.5)$$

This extension of the polynomial traction-separation law contains four parameters, two for normal separation  $(\delta_0^N, T_0^N)$  and two for tangential separation  $(\delta_0^T, T_0^T)$ .

The term  $D_{\max}$  is the largest value of damage according to eq. (2.5), which the cohesive element has experienced so far. It remains constant under unloading conditions. It is worth noting that in this case the traction is a linear function of the separation.

For pure normal separation, eq. (3.4) gives the same function as eq. (3.2).

The separation energy  $\Gamma_0$  can be determined for pure normal or tangential separation according to eq. (2.3), which leads to

$$\Gamma_0^N = \frac{9}{16} T_0^N \delta_0^N , \quad \Gamma_0^T = \frac{9}{16} T_0^T \delta_0^T \quad (3.6)$$

for eq. (3.4) and eq. (3.5), respectively.

### 3.1.2 Exponential TSL

The exponential stress potential for pure normal decohesion is of the following form:

$$\Phi = \frac{9}{16} T_0 \delta_0 \left[ 1 - \left( 1 + z \left( \frac{\delta^N}{\delta_0} \right) - \frac{1}{2} \alpha z^2 \left( \frac{\delta^T}{\delta_0} \right)^2 \right) \exp \left( -z \left( \frac{\delta^N}{\delta_0} \right) \right) \right] \quad (3.7)$$

The value of the constant factor  $z$  is  $z = 16e/9$  with  $e = \exp(1)$ . From eq. (3.7) the following stresses can be derived:

$$T^N = T_0 e \left[ z \left( \frac{\delta^N}{\delta_0} \right) - \frac{1}{2} \alpha z^2 \left( \frac{\delta^T}{\delta_0} \right)^2 \right] \exp \left( -z \left( \frac{\delta^N}{\delta_0} \right) \right) \quad (3.8)$$

and

$$T^T = T_0 e \left[ \alpha z \left( \frac{\delta^T}{\delta_0} \right) \right] \exp \left( -z \left( \frac{\delta^N}{\delta_0} \right) \right) \quad , \quad (3.9)$$

respectively. An extension for the application of shear fracture in conjunction with the second potential is described in [Xu and Needleman, 1994], but not implemented here. Unloading is not implemented in the exponential model as well; the damage is fully reversible. A sophisticated model for unloading in conjunction with eq. (3.8) is published in [Roe, 2001].

It is worth noting that the constant parameters of the model are chosen so that the cohesive energy at infinite separation is the same as for the polynomial TSL. That is, eq. (3.6) also holds for the exponential form. Since the TSL has a horizontal asymptote, the traction at  $\left( \frac{\delta^N}{\delta_0} \right) = 1$  is not zero, but equal to  $\left( \frac{T}{T_0} \right) = 0.105$ .

### 3.1.3 Partly constant TSL

The third TSL again is capable of shear fracture and unloading and can be applied to three-dimensional problems. In contradiction to the TSL's mentioned above, the tractions are of the form

$$T^N = T^N(\delta^N, \delta^T) = T_0^N f(\delta^N) g(\delta_{\max}^T) \quad T^T = T^T(\delta^T, \delta^N) = T_0^T f(\delta^T) g(\delta_{\max}^N) \quad (3.10)$$

$\delta_{\max}^T, \delta_{\max}^N$  are the maximum separation values occurred so far.

The implementation of this TSL has been done according to [Scheider, 2001a]. It is based on the law with a rectangular stress function  $T^N, T^T = \text{const}$  of Lin (summarized in [Lin, 1998]), shown in fig. 2.2b). Due to the implementation within ABAQUS, in which the cohesive elements are embedded in the stiffness matrix, a constant stress function is not possible, since the stiffness would be infinite as long as the maximum traction is not reached. A jump in the TSL would be inconsistent with the requirement of steady differentiability. That is why the jump at initial separation is replaced by a quadratic function.

To avoid convergence problems the jump at total separation  $\delta_0$  is also replaced by function which ensures a steady differentiable reduction of the traction up to the total loss of stress carrying capacity. A cubic function is used here.

The increase of the stress, constant term and decrease leads to the following approach of the TSL, both for the normal separation,  $\delta = \delta^N$ , and the tangential separation,  $\delta = \delta^T$ :

$$f(\delta) = \begin{cases} 2 \left( \frac{\delta}{\delta_1} \right) - \left( \frac{\delta}{\delta_1} \right)^2 & \delta < \delta_1 \\ 1 & \delta_1 < \delta < \delta_2 \\ 2 \left( \frac{\delta - \delta_2}{\delta_0 - \delta_2} \right)^3 - 3 \left( \frac{\delta - \delta_2}{\delta_0 - \delta_2} \right)^2 + 1 & \delta_2 < \delta < \delta_0 \end{cases} \quad (3.11)$$

In practise one can choose  $\delta_1$  very small without convergence problems, whereas the softening branch of the curve whose beginning is characterized by  $\delta_2$  must cover a broader range. For

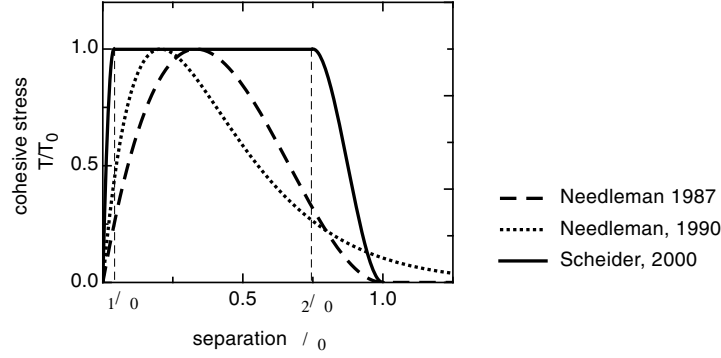


**Fig. 3.1:** Implemented traction separation functions (one dimensional illustration)

the computations proposed in [Scheider, 2001a] values of  $\delta_1 = 0.01$  and  $\delta_2 = 0.75$  have been chosen. In fig. 3.1 function eq. (3.11) is displayed with these values. If one sets  $\delta_1 = \delta_2 = 0.33$  then the curve is very similar to that according to [Needleman, 1987] — the softening curve is actually identically.

The cohesive energy for pure normal or tangential separation can be determined using eq. (2.3) with eq. (3.10) and eq. (3.11) by

$$\Gamma_0 = \int_0^{\delta_0} T(\delta) d\delta = T_0 \delta_0 \left( \frac{1}{2} - \frac{1}{3} \frac{\delta_1}{\delta_0} + \frac{1}{2} \frac{\delta_2}{\delta_0} \right) . \quad (3.12)$$

If from experiments the cohesive energy is known, then the maximum separation is given by

$$\delta_0 = \frac{2\Gamma_0}{T_0} \frac{1}{\left( 1 - \frac{2}{3} \frac{\delta_1}{\delta_0} + \frac{\delta_2}{\delta_0} \right)} . \quad (3.13)$$

The function  $g(\delta)$  in eq. (3.10) defines the connection between the normal traction and the tangential opening, and vice versa. There is no obvious physical foundation for a specific function. In the current implementation, a cubic decreasing function has been used:

$$g(\delta) = 2 \left( \frac{\delta}{\delta_0} \right)^3 - 3 \left( \frac{\delta}{\delta_0} \right)^2 + 1 \quad (3.14)$$

The normal traction for the models due to Scheider, eq. (3.10), and Tvergaard (1990), eq. (3.4), under a combined normal and tangential separation are shown in a contourplot, fig. 3.2. Given in the figure are the lines of equal normal tractions,  $T^N$ , with  $T_0^N = 1000$  MPa.

In this model unloading is defined to occur for normal and tangential tractions separately. If normal separation decreases, the normal traction decreases, too, with a linear function of the separation. Since the function  $g$  is only dependent on the maximum (shear-)separation, a decreasing  $\delta^T$  has no influence on the normal traction.

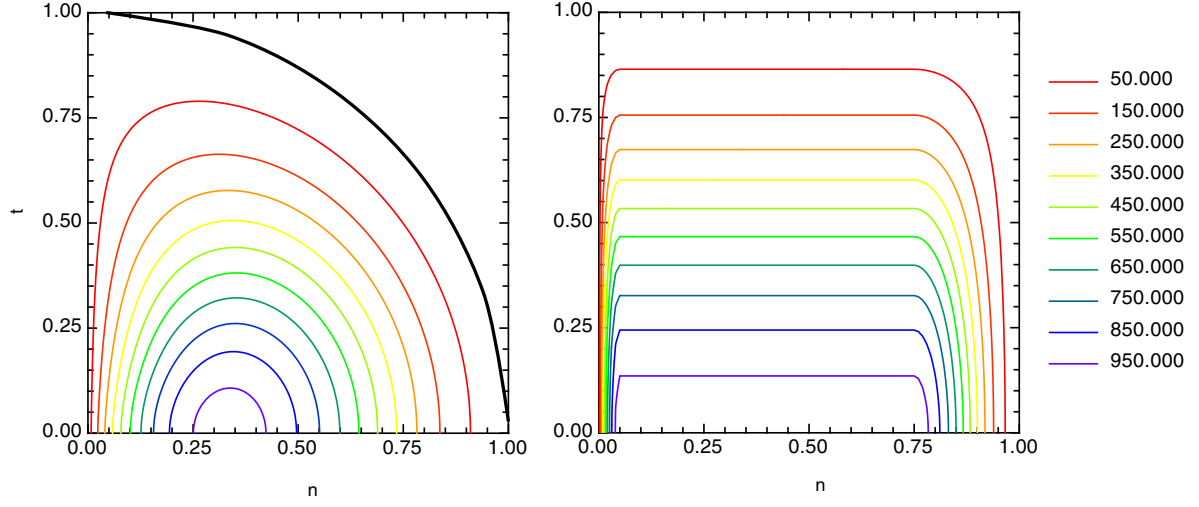


**Fig. 3.2:** Plot showing the lines of equal normal tractions under a combined normal and tangential separation a) for the TSL acc. to [Tvergaard, 1990]; b) acc. to Scheider.

The slope of the normal traction under unloading conditions is the initial slope of the function  $f(\delta^N = 0) = 2/\delta_1$ . For a mathematical formulation of the unloading behaviour one has to redefine eq. (3.10):

$$T^N = T^N(\delta^N, \delta^T) = T_0^N f^*(\delta^N) g(\delta_{\max}^T) \quad T^T = T^T(\delta^T, \delta^N) = T_0^T f^*(\delta^T) g(\delta_{\max}^N) \quad (3.15)$$

with

$$f^* = \begin{cases} 2 \left( \frac{\delta - \delta_{\max}}{\delta_1} \right) + \frac{T_{\max}^N}{T_0} & \delta < \delta_{\max} \\ f & \delta > \delta_{\max} \end{cases} \quad (3.16)$$

$T_{\max}^N$  is the traction at the maximum separation  $\delta_{\max}^N$ .

In the following table the tractions for all possible loading conditions are given. The derivation of a quantity with respect to  $\delta^N$  and to  $\delta^T$  are denoted by  $(\cdot)_{,N}$  and  $(\cdot)_{,T}$ , respectively.

	$T^T$ , Loading	$T^T$ , Unloading
$T^N$ , Loading	$T^N = T_0^N f(\delta^N) g(\delta_{\max}^T)$ $T^T = T_0^T f(\delta^T) g(\delta_{\max}^N)$ $T_{,N}^N = T_0^N f_{,N}(\delta^N) g(\delta_{\max}^T)$ $T_{,T}^N = T_0^N f(\delta^N) g_{,T}(\delta_{\max}^T)$ $T_{,N}^T = T_0^T f_{,N}(\delta^T) g(\delta_{\max}^N)$ $T_{,T}^T = T_0^T f(\delta^T) g_{,T}(\delta_{\max}^N)$	$T^N = T_0^N f(\delta^N) g(\delta_{\max}^T)$ $T^T = T_0^T \left[ 2 \frac{\delta^T - \delta_{\max}^T}{\delta_1} - \frac{T_{\max}^T}{T_0^T g(\delta_{\max}^T)} \right] g(\delta_{\max}^N)$ $T_{,N}^N = T_0^N f_{,N}(\delta^N) g(\delta_{\max}^T)$ $T_{,T}^N = 0$ $T_{,N}^T = T_0^T \left[ 2 \frac{\delta^T - \delta_{\max}^T}{\delta_1} - \frac{T_{\max}^T}{T_0^T g(\delta_{\max}^T)} \right] g_{,N}(\delta_{\max}^N)$ $T_{,T}^T = T_0^T \frac{2}{\delta_1} g_{,T}(\delta_{\max}^N)$
$T^N$ , Unloading	$T^N = T_0^N \left[ 2 \frac{\delta^N - \delta_{\max}^N}{\delta_1} - \frac{T_{\max}^N}{T_0^N g(\delta_{\max}^T)} \right] g(\delta_{\max}^T)$ $T^T = T_0^T f(\delta^T) g(\delta_{\max}^N)$ $T_{,N}^N = T_0^N \frac{2}{\delta_1} g_{,N}(\delta_{\max}^T)$ $T_{,T}^N = T_0^N \left[ 2 \frac{\delta^N - \delta_{\max}^N}{\delta_1} - \frac{T_{\max}^N}{T_0^N g(\delta_{\max}^T)} \right] g_{,T}(\delta_{\max}^T)$ $T_{,N}^T = 0$ $T_{,T}^T = T_0^T f_{,T}(\delta^T) g(\delta_{\max}^N)$	$T^N = T_0^N \left[ 2 \frac{\delta^N - \delta_{\max}^N}{\delta_1} - \frac{T_{\max}^N}{T_0^N g(\delta_{\max}^T)} \right] g(\delta_{\max}^T)$ $T^T = T_0^T \left[ 2 \frac{\delta^T - \delta_{\max}^T}{\delta_1} - \frac{T_{\max}^T}{T_0^T g(\delta_{\max}^T)} \right] g(\delta_{\max}^N)$ $T_{,N}^N = T_0^N \frac{2}{\delta_1} g_{,N}(\delta_{\max}^T)$ $T_{,T}^N = 0$ $T_{,N}^T = 0$ $T_{,T}^T = T_0^T \frac{2}{\delta_1} g_{,T}(\delta_{\max}^N)$

### 3.1.4 Aspects of numerical implementation

For the calculation of the stiffness of the cohesive element, i.e. the rate of the load in dependence of the displacement, it is necessary to evaluate the derivative of the normal and tangential traction to the separations. If the equation for the traction contains the damage  $D$  as shown in principal in eq. (2.6), e.g. eq. (3.4), this has been done by partial derivative. The derivative of the tractions then leads to

$$\frac{dT^N}{d\delta^N} = \frac{\partial T^N}{\partial \delta^N} + \frac{\partial T^N}{\partial D} \frac{\partial D}{\partial \delta^N} \quad \text{and} \quad \frac{dT^N}{d\delta^T} = \frac{\partial T^N}{\partial \delta^T} + \frac{\partial T^N}{\partial D} \frac{\partial D}{\partial \delta^T} \quad . \quad (3.17)$$

The derivative of the shear traction is analogous. For threedimensional analyses where two tangential separations exist, the derivative has to be performed with respect to each of these separations,  $\delta^{Ti}$  ( $i = 1, 2$ ), which leads to

$$\frac{dT^N}{d\delta^{Ti}} = \frac{\partial T^N}{\partial \delta^T} \frac{\partial \delta^T}{\partial \delta^{Ti}} + \frac{\partial T^N}{\partial D} \frac{\partial D}{\partial \delta^T} \frac{\partial \delta^T}{\partial \delta^{Ti}} \quad . \quad (3.18)$$

The shear tractions for the 3D case have to be split into the directions of  $\delta^{T1}, \delta^{T2}$  before the derivative is executed:

$$T^{T1} = T^T \frac{\delta^{T1}}{\delta^T} \quad \text{and} \quad T^{T2} = T^T \frac{\delta^{T2}}{\delta^T} \quad (3.19)$$

The derivative of the shear tractions to the tangential separations thus leads to

$$\frac{dT^{T1}}{d\delta_1^{T1}} = \left( \frac{\partial T^T}{\partial \delta^T} \frac{\partial \delta^T}{\partial \delta_1^{T1}} + \frac{\partial T^T}{\partial D} \frac{\partial D}{\partial \delta^T} \frac{\partial \delta^T}{\partial \delta_1^{T1}} \right) \frac{\delta^{T1}}{\delta^T} + \frac{T^T}{\delta^T} \left( 1 - \left( \frac{\delta^{T1}}{\delta^T} \right)^2 \right) \quad . \quad (3.20)$$

and

$$\frac{dT^{T1}}{d\delta_2^T} = \left( \frac{\partial T^T}{\partial \delta^T} \frac{\partial \delta^T}{\partial \delta^{T2}} + \frac{\partial T^T}{\partial D} \frac{\partial D}{\partial \delta^T} \frac{\partial \delta^T}{\partial \delta^{T2}} \right) \frac{\delta^{T1}}{\delta^T} \quad (3.21)$$

The derivatives of  $T^{T2}$  with respect to  $\delta^{T1}$  and  $\delta^{T2}$  are analogous. It is worth noting that for the three-dimensional case a reverse loading (see the so-called *negative loading case* in chapter 2.4.2) is not possible, since the total tangential separation is always positive. Nevertheless, a local unloading in tangential direction can occur.

The separations are calculated in every increment for all cohesive elements at the integration points. When the separation energy according to eq. (3.6) or eq. (3.12) is reached (or the respective separations), the element has failed at this point<sup>1</sup>. The contribution of the integration point to the stiffness vanishes and the point gets the status "failed". An integration point that has lost its stiffness once, can never get another status.

## 3.2 Element library

User defined elements have been developed for two- and three-dimensional models. Since they behave like contact elements (but contrary to those they may be stressed under tension loading), they have one dimension less than the surrounding continuum elements. Even though the cohesive element has no volume in the unloaded and undamaged state, they will be called 3D cohesive element in the following, the elements for twodimensional problems will be called 2D cohesive elements, respectively.

The 2D cohesive elements have four nodes with a linear displacement formulation. Elements are implemented for plane and for axisymmetric problems. There is no difference between plane stress and plane strain elements, since the stress in the third direction does not influence the behaviour of the cohesive element. The difference between those two element types is the calculation of the integration point area: While the area of plane elements is calculated by the half length of the element times its thickness, the integration point area of axisymmetric elements depends on the distance from the rotation axis. A problem arises when plane stress elements are used: The thickness of the continuum element can not be taken into account, since the actual thickness of the element is not handed to the user element subroutine.

Contrary to the linear formulation of the 2D cohesive elements, the three-dimensional elements are variable node elements; they can be built using eight nodes and a linear displacement formulation or with quadratic displacements and 16 or 18 nodes. The stresses are calculated similar to the 2D cohesive elements at the integration points according to the TSL. Possible numbers for the integration points per element are 4 or 9. Theoretically any combination of node and integration point number is possible, but a linear element with nine integration points is not very useful. A quadratic element with 4 integration points might lead to zero energy modes but the experience shows that this does not happen in a crack propagation analysis.

Elements are shown in fig. 3.3. In the undeformed state every two nodes share the same coordinates, but in the drawing they are plotted with a short distance for clarification.

<sup>1</sup>In the exponential separation law, eq. (3.8), this energy is reached at infinitum. Internal to the program the element stiffness is set to zero at  $\delta = 10\delta_0$ . At this separation more than 99% of the total energy is dissipated.

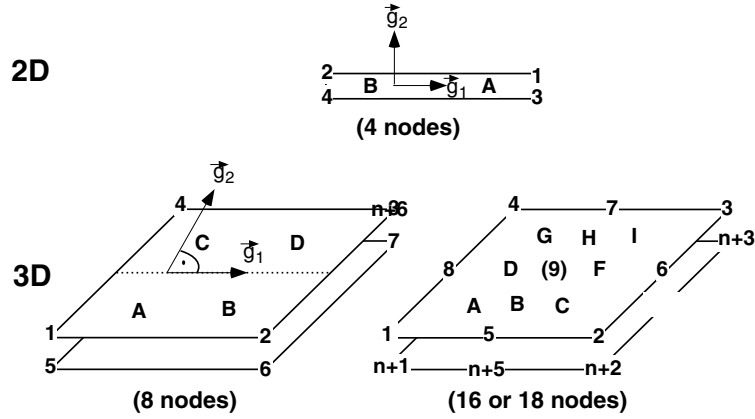


**Fig. 3.3:** Element node and integration point positions for the two- and threedimensional element. The configuration for the 3D 8 node and 16/18 node elements are shown separately.

### 3.3 Local coordinate system

The following section regards to the threedimensional cohesive element. All explanations can be applied to the 2D element as well.

For the quantitative evaluation of separation of the opposite cohesive surfaces one face is called *upper* and the other *lower* surface, but these names are chosen arbitrarily and only used for the distinction in the text. In the undeformed state both faces are at the same geometrical position. The separation can be due to sliding or "tangential opening" (which is shear fracture), normal opening (Mode I fracture) or any combination of these two.

The local coordinate system is constructed in the following way: The local direction  $\vec{g}_1$  is the direction between the edge bisector between nodes N1 and N4 to the edge bisector between nodes N2 and N3, cf. fig. 3.3. The direction  $\vec{g}_2$  is defined by the orthogonal part of the straight line between the edge bisector  $\overline{K1 K2}$  and  $\overline{K3 K4}$ . The face normal can then be calculated by the crossproduct  $\vec{g}_3 = \vec{g}_1 \times \vec{g}_2$ . A definition of the local coordinate system as a field variable, which is possible using the Jakobi matrix, has not been used. The separations in the direction of  $\vec{g}_1$  are called  $\delta^{T1}$ , those in the direction of  $\vec{g}_2$  are called  $\delta^{T2}$ . The local coordinates in the respective directions are named  $\xi$  and  $\eta$ . The coordinate value in the third direction is  $\zeta$ . The field variable of the separations due to "tangential opening" in the two coordinate directions,  $\delta^{T1}$ ,  $\delta^{T2}$ , and normal opening,  $\delta^N$ , are  $(\delta^{T1}(\xi, \eta), \delta^{T2}(\xi, \eta), \delta^N(\xi, \eta))$ .

There is no difference for the cohesive element, which of either surface is moving absolutely. From this it follows that neither the upper nor the lower face can be the reference face for the coordinate system. Instead of these two other possibilities for the definition of the local coordinate system are implemented:

1. The original position of the cohesive element is taken as the reference for the coordinate system. This is analogous to the theory of small deformations.
2. Analogous to the theory of large deformation the coordinate system is moving with the element using a mid section face, that is as the bisector between upper and lower surface.



In fig. 3.4 the difference is visible with regard to a rotation of a 2D element: While definition 1 with its coordinate system  $(\xi_1, \zeta_1)$  leads to a partly tangential opening in direction  $\xi_1$ , the element is separated under pure Mode I (direction  $\zeta_2$ ) using the definition 2, coordinate system  $(\xi_2, \zeta_2)$ .

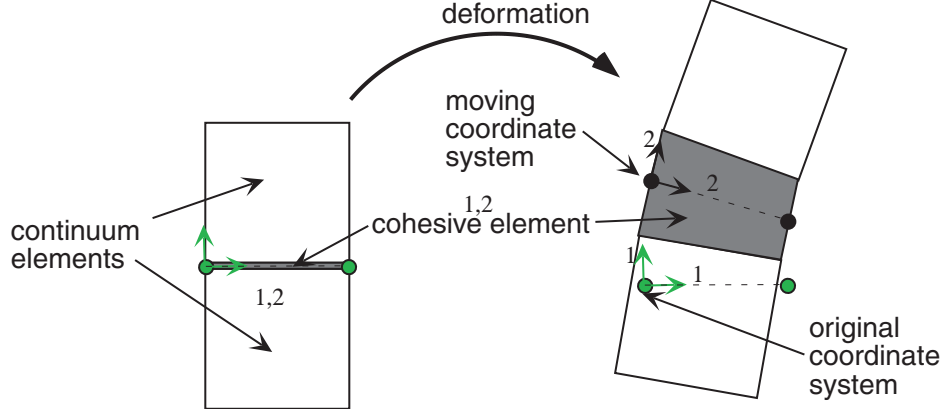


**Fig. 3.4:** Definition of the local coordinate system within the cohesive element.

### 3.4 Energy principle for the cohesive element

The stiffness matrix for the cohesive element can be derived based upon the principle of virtual work. Since  $\delta$  usually means the variation of a quantity, the separation will be denoted as  $[\mathbf{u}]$  in this section for minimizing the risk of confusion.

The virtual work of stresses for the cohesive element is defined by

$$\delta\Pi_i = \int \mathbf{t} \cdot \delta[\mathbf{u}] dA \quad , \quad (3.22)$$

where  $\mathbf{t}$  is the vector of the cohesive stresses acting on the separations.

In the following a compatible approach for the coordinates and the separations  $[\mathbf{u}]$ ,  $\delta[\mathbf{u}]$  according to the finite element formulation of the connected continuum elements is constructed (linear, quadratic, two- or three-dimensional, etc.). The displacements  $[\mathbf{u}]$  are replaced by the product of the matrix of shape functions  $\mathbf{V}_u$  and the displacements at the nodes  $\mathbf{u}_e$ :

$$\mathbf{u} = \mathbf{V}_u \cdot \mathbf{u}_e \quad (3.23)$$

The content of  $\mathbf{V}_u$  is

$$V_{ij} = \begin{pmatrix} f_1 & 0 & 0 & f_2 & 0 & 0 & \dots & f_n & 0 & 0 \\ 0 & f_1 & 0 & 0 & f_2 & 0 & \dots & 0 & f_n & 0 \\ 0 & 0 & f_1 & 0 & 0 & f_2 & \dots & 0 & 0 & f_n \end{pmatrix} \quad (3.24)$$

Using eq. (3.23), eq. (3.22) leads to

$$\delta\Pi_i = \delta[\mathbf{u}_e] \cdot \int \mathbf{V}_u^T \cdot \mathbf{t} \, dA \quad (3.25)$$

Since the cohesive stresses used in eq. (3.22) are nonlinear functions of the displacements, the nodal displacements cannot be extracted from the integral, and a linear system of equations can not be set up. The tangential stiffness matrix of the incremental solution can be calculated with eq. (3.25) using the total differential of the tractions

$$d\mathbf{t} = \frac{\partial \mathbf{t}}{\partial \mathbf{u}} \cdot d\mathbf{u} \quad (3.26)$$

In practise the difference  $\Delta\mathbf{u}$  is used instead of  $d\mathbf{u}$ . The total displacement at the time  $t + \Delta t$  is then given by  $\mathbf{u}^{t+\Delta t} = \mathbf{u}^t + \Delta\mathbf{u}$ . With the differential formulation the incremental system of equations writes:

$$\mathbf{K} \cdot \Delta[\mathbf{u}_e] = \int \mathbf{V}_u^T \cdot \frac{\partial \mathbf{t}}{\partial [\mathbf{u}]} \cdot \mathbf{V}_u \, dA \cdot \Delta[\mathbf{u}_e] \quad (3.27)$$

The integration of eq. (3.27) is done numerically using the Gauss integration algorithm. With that the integral leads to

$$\mathbf{K} = \int \mathbf{V}_u^T \cdot \frac{\partial \mathbf{t}}{\partial [\mathbf{u}]} \cdot \mathbf{V}_u \, dA = \sum_i \left( \mathbf{V}_u^T \cdot \frac{\partial \mathbf{t}}{\partial [\mathbf{u}]} \cdot \mathbf{V}_u \right) \Big|_i w_i J_i \quad (3.28)$$

$w_i$  are the weight function for the Gauss integration,  $J_i$  is the Jacobian determinant of the cohesive element at the specific Gauss point. As already mentioned, the cohesive element itself has only two dimensions, so the Jacobian determinant is calculated from the matrix

$$\mathbf{J} = \begin{pmatrix} \frac{\partial x}{\partial \xi} & \frac{\partial y}{\partial \xi} \\ \frac{\partial x}{\partial \eta} & \frac{\partial y}{\partial \eta} \end{pmatrix} \quad (3.29)$$

The Jacobian determinant can be set up using the undeformed or the deformed coordinates according to the theory of small or large deformations. Independently to this the element coordinate system (chapter 3.3) can be defined in the reference plane or in the deformed bisector plane, according to small or large rotations.

Due to the sparse matrix  $\mathbf{V}_u$ , glrefeq.ansatzmatrix, the term in parenthesis of eq. (3.28) can be calculated easily. After back transformation of the local stresses and separations to the global





## Chapter 4

# ABAQUS input for the cohesive element

The element definition within ABAQUS is done using the command `ELEMENT`. At this time three elements, U1 (cohesive element for axisymmetric problems), U2 (plane cohesive element) and U5 (cohesive element for three-dimensional problems) are implemented.

With the parameter `ELEMENT,TYPE=` the specific type (U1, U2 or U5) is set up. The input is done by

```
ELEMENT, TYPE=U1|U2|U5 [,ELSET=name]
element nr, node1, node2, ..., nodeN
```

The arrangement of the nodes in the specific elements is shown in fig. 3.3.

Beside the element definition there are three additional commands required in the ABAQUS input file for the crack propagation analysis with cohesive elements. At first the element types must be announced to the program. This is done by

```
USER ELEMENT, TYPE=eltype_name, NODES=number_of_nodes,
PROPERTIES=real_props, IPROPERTIES=integer_props,
COORDINATES=number_of_dofs, VARIABLES=number_of_outputvariables
```

The values required for the parameters are given in the following table:

	U1 (axisymm.)	U2 (plane ele- ment)	U5 (3D element)
TYPE	U1	U2	U5
NODES	4	4	8 – 18
PROPERTIES	5/7	5/7	4/6
IPROPERTIES	2	2	3
COORDINATES	2	2	3
VARIABLES	14/18	14/18	5 x NODES

As already mentioned in chapter 3.2, the node number of element type U5 is variable and can be 8, 16 or 18. The number of properties used in a 2D analysis is 5 for the polynomial and the exponential model and 7 for the model of Scheider. For a 3D analysis one property, the thickness, is omitted.

The number of output variables is 14 for plain or axisymmetric elements together with the polynomial or the exponential model, 18 variables are required for the model due to Scheider.

The input of the cohesive material parameters is done for the plane and axisymmetric elements by

```
UEL PROPERTY,ELSET=elset_name
delta_N, delta_T, traction_N, traction_T, thickness, [ delta_1, delta_2,] model
coord_flag
```

The parameter `model` defines the TSL and is an integer number. Here 1 means the TSL due to [Tvergaard, 1990] (polynomial approach), 2 is due to [Needleman, 1990] (exponential approach) and 3 defines the model due to [Scheider, 2001a].

`coord_flag` can have the values 0 and 1. 0 means that the local coordinate system is fixed at the reference plane of the cohesive element, with `coord_flag=1` the actual configuration is used for the coordinate system, cf. chapter 3.3.

For the models 1 and 2 the parameters `delta_1` and `delta_2` are not needed and are therefore omitted<sup>1</sup> The value for `delta_T` can not be arbitrarily chosen for model 2, but is defined by  $\delta^T = \frac{T^T}{T^N} \delta^N$ . The input of this parameter is therefore obsolete. In addition, the parameter `thickness` is not used for the axisymmetric elements. Nevertheless, either of the latter parameters must be set.

The input of the element properties for the 3D element is very similar to the 2D element:

```
UEL PROPERTY,ELSET=elset_name
delta_N, delta_T, traction_N, traction_T, delta_1, delta_2, model, coord_flag
number_of_gausspoints
```

There is no thickness to be put in for the 3D element. The `number_of_gausspoints` can be 4 or 9. In addition the value can be 0 for a full integration (4 integration points for elements with linear formulation and 9 integration points for elements with a quadratic formulation) and -1 (always 4 integration points), respectively.

Beside the commands `UEL PROPERTY` and `USER ELEMENT` a command is required which specifies the position of the FORTRAN source code file for the user element routine in the directory tree. This is done by

```
USER SUBROUTINE, INPUT=quelldatei.f
```

An example input file for the verification model (chapter 6) is given in appendix B.

---

<sup>1</sup>Caution: Since always a set of 8 values must be in one line, the input of `coord_flag` has to be written on the same line as `model`.

## Chapter 5

# Results output

The definition of `*USER ELEMENT, VARIABLES=...` leads to 14 values per 2D–element for each increment. For the 3D elements 10 values per integration point are printed (i.e. 40 or 90 values per element). The variables can be post processed by `abaqus post` only by the definition of curves. In addition, the output to the `.dat` file is possible. The command for the printing of the variables to that file is

```
EL PRINT,ELSET=cohesive element group
SDV1, ..., SDVn
```

The command for the output to the results file (Suffix `.fil`) is

```
EL FILE,ELSET=cohesive element group
SDV
```

The following variables are defined for the 2D cohesive elements:

variable	meaning
SDV1	normal separation $\delta^N$ (int. point A)
SDV2	tangential separation $\delta^T$ (int. point A)
SDV3	normal separation $\delta^N$ (int. point B)
SDV4	tangential separation $\delta^T$ (int. point B)
SDV5	normal stress $T^N$ (int. point A)
SDV6	tangential stress $T^T$ (int. point A)
SDV7	normal stress $T^N$ (int. point B)
SDV8	tangential stress $T^T$ (int. point B)
SDV9	status of damage (int. point A)
SDV11	<b>Model 1:</b> max. absolute separation $D$ experienced so far (int. point A)
	<b>Model 3:</b> max. normal separation $\delta_{\max}^N$ experienced so far (int. point A)
SDV13	<b>Model 3:</b> max. tangential separation $\delta_{\max}^T$ experienced so far (int. point A)
SDV15	Shift of the origin of the tangential TSL for positive tractions, $\delta^{+0}$ (int. point A)
SDV17	Shift of the origin of the tangential TSL for negative tractions, $\delta^{-0}$ (int. point A)
SDV10 ... SDV18	as SDV9 ... SDV17 for int. point B

The variables SDV9 . . . SDV18 are used internally and are of little importance for the post processing. Variables SDV14 . . . SDV18 are required only for model 3.

The variables SDV9 and SDV10, respectively, specify the status regarding failure of the element. When SDV9=-1, the cohesive element has lost its stiffness and the crack is advanced one integration point. SDV9=0 means that the integration point actually experiences local unloading (not available for model 2). For model 3 there is a distinction between the status of normal and tangential separation, both of which are given in SDV9. The value of the variable consists of two alphanumeric characters in front of the decimal point (MN.000). The meaning of M and N is given in the table below:

value	meaning
0	unloading
1	loading, maximum stress $T_0$ is not yet reached
2	loading, region of constant stress
3	loading, softening region

If the element fails due to a separation greater than the maximum separation, it gets the status -1 (no distinction between normal and shear state).

For the 3D elements the output consists of 10 variables per integration points, which are stored sequentially for all integration points of the element. The following table therefore gives only the meaning of the variables for one integration point.

variable	meaning
SDV1	normal separation $\delta^N$
SDV2	tangential separation, direction 1: $\delta^{T1}$
SDV3	normal separation, direction 2: $\delta^{T2}$
SDV4	normal spannung $T^N$
SDV5	tangential spannung, direction 1: $T^{T1}$
SDV6	tangential spannung, direction 2: $T^{T2}$
SDV7	<b>Model 1:</b> status of damage <b>Model 3:</b> status of damage in normal direction
SDV8	<b>Model 3:</b> status of damage in tangential direction
SDV9	<b>Model 1:</b> max. absolute separation $D$ experienced so far <b>Model 3:</b> max. normal separation experienced so far $\delta_{\max}^N$
SDV10	<b>Model 3:</b> max. tangent. separation experienced so far $\delta_{\max}^T$

The directions T1 and T2 confer to the directions  $\vec{g}_1$  and  $\vec{g}_2$  defined in chapter 3.2. The maximum tangential separation is defined by the norm of both components  $\delta^{T1}$  and  $\delta^{T2}$ .

The status of the damage for the 3D elements of model 3 is divided in normal and tangential direction (SDV7 and SDV8). The value of these variables can be:

value	meaning
0	unloading
1	loading, maximum stress $T_0$ is not yet reached
2	loading, region of constant stress
3	loading, softening region
-1	total failure



## Chapter 6

# Verification: Three element test for tangential separation with alternating loading direction

In the following a three element test as shown in fig. 6.1 consisting of two 2D continuum elements (plane strain) and one cohesive element under  $45^\circ$  with respect to the loading direction is analyzed. The cyclic  $y$ -displacement of the nodes N1 and N2 is plotted in fig. 6.2a. The nodes N7 and N8 are fixed in the  $y$ -direction, the  $x$ -displacement of node N7 is fixed, too. It shall be investigated, how The behaviour of the traction and separation under cyclic loading is investigated using the TSL of eq. (3.11).

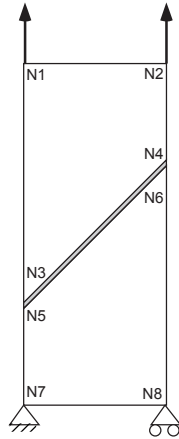


**Fig. 6.1:** 3 element test for the verification of the behaviour of the cohesive element (grey shaded between the two continuum elements) at alternating loading direction

The material of the continuum elements follows an potential elastic plastic law with a yield limit of 100 MPa and a hardening exponent of  $n = 5$ . The cohesive element has a normal and tangential traction of  $T_0^N = 160\text{MPa}$  and  $T_0^T = 80\text{MPa}$ , respectively. The maximum separation is  $\delta_0^N = 0.05\text{mm}$  and  $\delta_0^T = 0.2\text{mm}$ , respectively. The TSL used is the model 3, [Scheider, 2001a], with the additional parameter  $\delta_1 = 0.01\delta_0$  and  $\delta_2 = 0.75\delta_0$ .

Since in the cohesive element the separation is almost solely tangential — the normal stresses

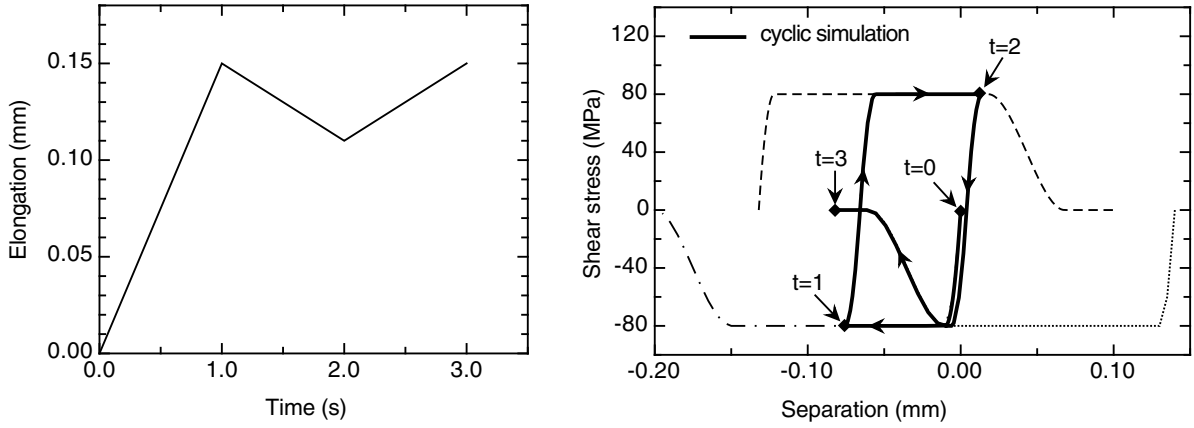


**Fig. 6.2:** a: cyclic prescribed displacement for the shear test; b: curve of the tangential traction with respect to the separation

stay below the maximum traction  $T_0$  —, the total shear separation  $\delta_0^T$  is available up to total failure. In fig. 6.2b the traction separation curve is shown for the cyclic loading. Up to time  $t = 1$  the damage increases to a value of about 38%. The shear traction (and the associated separation) are negative during that time. The full separation curve (up to  $\delta^T = \delta_0^T$ ) in that direction is shown in the figure with a dashdotted line.

When the prescribed displacement is reversed, the value of separation decreases, the stress in the element becomes positive and the damage also increases although the absolute value of separation decreases. At  $t = 2$  the amount of damage is 72%. The loading path in terms of traction–separation follows the curve shown with a dashed line in figure fig. 6.2b. it can be seen, that the origin of the curve is shifted to the negative direction according to eq. (2.7).

After a second change in the loading direction, the separation follows the dotted damage curve, and the traction stays constant until the damage has reached a value of 75%, which is also the value of  $\delta_2$ . When the loading increases further, the traction decreases according to the cubic part of the TSL. The total failure is reached at  $t = 2.785$ . The total energy dissipated by that loading process, calculated by the integral of the traction with respect to the separation, is 13.7 N/mm. This is exactly the value of the separation energy  $\Gamma_0$ , which can be calculated using eq. (3.12).

# Bibliography

- [Barenblatt, 1962] Barenblatt, G. (1962). The mathematical theory of equilibrium cracks in brittle fracture. *Advances in Applied Mechanics*, 7:55–129.
- [Carpinteri, 1986] Carpinteri, A. (1986). *Mechanical damage and crack growth in slits*. Martinus Nijhoff Kluwer.
- [Chaboche et al., 1997] Chaboche, J., Girard, R., and Levasseur, P. (1997). On the interface debonding models. *International Journal of Damage*, 6:220–257.
- [de Andres et al., 1999] de Andres, A., Perez, J., and Ortiz, M. (1999). Elastoplastic finite element analysis of three dimensional fatigue crack growth in aluminum shafts subjected to axial loading. *Int. J. Sol. Struct.*, 36:2231–2258.
- [Dugdale, 1960] Dugdale, D. S. (1960). Yielding of steel sheets containing slits. *J. Mech. Phys. Solids*, 8:100–104.
- [Gurson, 1977] Gurson, A. L. (1977). Continuum theory of ductile rupture by void nucleation and growth: Part i - yield criteria and flow rules for porous ductile media. *J. Eng. Mater. Tech.*, 99:2–15.
- [Hibbitt et al., 1998] Hibbitt, Karlsson, and Sorensen (1998). *ABAQUS Theory manual 5.8*. Hibbitt, Karlsson & Sorensen.
- [Hillerborg et al., 1976] Hillerborg, A., Modeer, M., and Petersson, P. (1976). Analysis of crack formation and crack growth in concrete by means of fracture mechanics and finite elements. *Cement Concrete Res.*, 6:773–782.
- [Lin, 1998] Lin, G. (1998). *Numerical investigation of crack growth behaviour using a cohesive zone model*. PhD thesis, TU Hamburg-Harburg, Geesthacht.
- [Lin et al., 1996] Lin, G., Cornec, A., and Schwalbe, K.-H. (1996). Cohesive zone model for ductile fracture - comparison of prediction with experiment. In *Proceedings of the 11th Biennial European Conference on Fracture*, volume I, pages 101–106. The Chameleon Press Ltd. London.
- [Needleman, 1987] Needleman, A. (1987). A continuum model for void nucleation by inclusion debonding. *J. Appl. Mech.*, 54:525–531.
- [Needleman, 1990] Needleman, A. (1990). An analysis of decohesion along an imperfect interface. *International Journal of Fracture*, 42:21–40.

- [Petersson, 1981] Petersson, P. E. (1981). Crack growth and development of fracture zones in plain concrete and similar materials. Technical report, Division of Building Materials, Lund Institute of Technology.
- [Rice, 1968] Rice, J. (1968). A path independent integral and the approximate analysis of strain concentrations by notches and cracks. *J. appl. Mech.*, 35:379–386.
- [Roe, 2001] Roe, K. L. (2001). *A cohesive zone model for fatigue crack growth simulation*. PhD thesis, Purdue University.
- [Scheider, 2001a] Scheider, I. (2001a). *Bruchmechanische Bewertung von Laserschweiveverbindungen durch numerische Riffortschrittsimulation mit dem Kohsivzonenmodell*. PhD thesis, TU Hamburg-Harburg, Geesthacht.
- [Scheider, 2001b] Scheider, I. (2001b). Simulation of cup-cone fracture in round bars using the cohesive zone model. In *First M.I.T. conference on Computational Fluid and Solid Mechanics*, pages 460–462.
- [Schwalbe and Cornec, 1994] Schwalbe, K.-H. and Cornec, A. (1994). Modelling crack growth using local process zones. Technical report, GKSS research centre, Geesthacht.
- [Siegmund and Brocks, 1998] Siegmund, T. and Brocks, W. (1998). Tensile decohesion by local failure criteria. *Technische Mechanik*, Band 18:261–270.
- [Siegmund et al., 1999] Siegmund, T., Brocks, W., Heerens, J., Tempus, G., and Zink, W. (1999). Modeling of crack growth in thin sheet aluminium. In *ASME Int. Mechanical Engineering Congress and Exposition: Recent Advances in Solids and Structures*, pages 15–22.
- [Tvergaard, 1990] Tvergaard, V. (1990). *Material failure by void growth to coalescence*, pages 83–151. Academic Press.
- [Tvergaard and Hutchinson, 1992] Tvergaard, V. and Hutchinson, J. W. (1992). The relation between crack growth resistance and fracture process parameters in elastic-plastic solids. *J. Mech. Phys. Solids*, 40:1377–1397.
- [Xu and Needleman, 1994] Xu, X. and Needleman, A. (1994). Numerical simulations of fast crack growth in brittle solids. *J. Mech. Phys. Solids*, 42:1397–1434.

# Appendix A

## Program structure

The FORTRAN subroutine for the user element must be named `UEL` and has several arguments. The most important arguments are the nodal coordinates `COORDS`, the displacements `U` of the cohesive element and the internal variables, which can be assigned and manipulated by their names `SDV(i)`. The important output parameters are the element stiffness matrix `AMATRIX` and the load vector `RHS`, respectively. In `UEL`, first the input parameters and other variables are initialised, then the separations at the nodes `UX(i)`, `UY(i)` and `UZ(i)`<sup>1</sup> and the coordinates of the midplane (`X(i)`, `Y(i)` and `Z(i)`<sup>1</sup>), respectively, are calculated in global coordinates from the displacements of the adjacent nodes. The separations and material parameters are then passed to another subprogram, which depends on the element type (`U1/U2`: `CZE2D`, `U5`: `CZE3D5`). The proceeding in these routines is different in several ways. In both subroutines the normal and tangential separation are calculated in a element local coordinate system. These values are passed for each integration point to another subroutine (`2D`: `POTENT`, `3D`: `POT3D`), in which the normal and tangential tractions, `TN` and `TT`, respectively, and their derivatives, (`DTNDUN` etc.), are determined. These variables are returned to the calling subroutines, which calculate the stiffness matrix and the right hand side vector based on their values.

The structure of the subroutines is given in the following:

### A.1 For the 3D-cohesive elements:

- Determination of the separation `UX`, `UY`, `UZ` and the coordinates `X`, `Y`, `Z` (this is performed identically for the 2D and 3D elements in routine `UEL`)
- Passing of these variable to the subroutine `CZE3D5`
- Calculation of the local unit vectors `G1`, `G2`, `G3`, and the transformation matrix `ALPHA`, respectively.
- DO loop executed for every integration point
  - Calculation of the integration point displacement `UGP` using eq. (3.23). The integration point coordinates are calculated analogous.
  - Calculation of the Jacobian determinante at the integration point `XJDET` according to eq. (3.29)

---

<sup>1</sup>for the 3D cohesive element

- Transformation of the integration point displacements (components UN, UT1 and UT2)
  - Determination of the stresses and their derivatives within the subroutine POT3D
  - Backtransformation of the stresses and their derivatives
  - Calculation of the stiffness matrix  $\mathbf{K}$  (array AMATRX) using eq. (3.28)
  - Calculation of the global load vector  $\mathbf{f}$  (array RHS) using eq. (3.33)
- Assignment of the remaining values in RHS and AMATRX, respectively, since the components are calculated at the midsurface but have to be given for the nodes at the top and the bottom surface.

## A.2 For the 2D cohesive elements:

- Determination of the separation UX, UY, UZ and the coordinates X, Y, Z (this is performed identically for the 2D and 3D elements in routine UEL)
- Passing of these variable to the subroutine CZE3D5
- Determination of the angle with respect to the global x-axis THET
- Calculation of the transformation maxtrix (global  $\leftrightarrow$  local)  $\begin{pmatrix} XT1 & XT2 \\ XN1 & XN2 \end{pmatrix}$
- Determination of the integration point area AREAA (integration point A) and AREAB (integration point B)<sup>3</sup>
- Transformation of the separation at the nodes into the local coordinate system
- Calculation of the local separation at the integration points  
Integration point A: UNA, UTA; Integration point B: UNB, UTB
- Calculation of the stresses in the local coordinate system in subroutine POTENT based on the separation law chosen
- Calculation of the forces (local coordinate system) (FNA, FTA, FNB, FTB) by multiplying the integration point area with the stresses.
- Calculation of the forces at the nodes in the local coordinate system (FNALP, FTALP, FNBET, FTBET) based on the balance of load and momentum.
- Back transformation into the global coordinate system using the transformation matrix.

---

<sup>3</sup>For the plane elements the area of one integration point is just half of the element length multiplied by the thickness. For the axisymmetric elements the thickness can be calculated by  $t_A = 2\pi(3/4r_A + 1/4r_B)$  and  $t_B = 2\pi(3/4r_B + 1/4r_A)$ , respectively.

# Appendix B

## Inputfile for the verification example

```
*HEADING
2 Element Test with tangential separation with alternating loading direction (twodimensional)
*****
*USER ELEMENT,TYPE=U2,NODES=4,PROPERT=7,IPROP=2,COORDI=2,VAR=14
1,2
*****
*NODE, SYSTEM=R
1, .000000000E+00, .000000000E+00, .000000000E+00
2, .100000000E+01, .100000000E+01, .000000000E+00
3, .000000000E+00, .200000000E+01, .000000000E+00
4, .100000000E+01, .200000000E+01, .000000000E+00
5, .000000000E+00, .000000000E+00, .000000000E+00
6, .100000000E+01, .100000000E+01, .000000000E+00
7, .000000000E+00,-.200000000E+01, .000000000E+00
8, .100000000E+01,-.200000000E+01, .000000000E+00
*ELEMENT,TYPE=CPE4 ,ELSET=E0000001
1, 1,2,4,3,
2, 5,7,8,6,
*ELEMENT,TYPE=U2 ,ELSET=E0000002
11, 2,1,6,5,
*SOLID SECTION,ELSET=E0000001,MATERIAL=M0001001
*MATERIAL,NAME=M0001001
*ELASTIC
.210000E+06, .300
*PLASTIC
.100000000E+03, .000000000E+00
.170000000E+03, .595170000E-02
.240000000E+03, .367744000E-01
.310000000E+03, .134853100E+00
.380000000E+03, .375500800E+00
.450000000E+03, .876562500E+00
.520000000E+03, .180801920E+01
.590000000E+03, .340159190E+01
.660000000E+03, .596034560E+01
.730000000E+03, .986829330E+01
.800000000E+03, .156000000E+02
*****
*UEL PROPERTY,ELSET=E0000002
.0500 , .2000 , 160.0 , 80.0 , 1.000 , .5000E-01, .750, 3
```





```
*BOUNDARY,OP=MOD
TOP,2,, 0.1500
*NODE PRINT,SUM=NO
U,RF
*****
*EL PRINT,ELSET=E0000002,SUM=NO
SDV1,SDV2,SDV3,SDV4,SDV5,SDV6,SDV7,SDV8
*****
*END STEP
```